Supplementary Information

1. The effect of the $\delta^{13}C(CH_4)$ seasonal cycle

CH_4 and $\delta^{13}C(CH_4)$ undergo seasonal cycles (Miller et al., 2002, Tyler et al., 2007, Dugoklencky et al., 2009), which are recorded in the upper firn. However, the inverse model cannot reconstruct the seasonal signal (see: Wang et al., 2011 for further discussion) thus it has to be assessed separately. The amplitude of the seasonal signal at the SH sites is very small and thus does not significantly affect the firn profiles from Antarctica. Therefore, the sensitivity to seasonality was only examined for the NH sites using the model in the forward mode. Model runs were performed for an atmospheric scenario with (Fig. S1: black lines) and without (Fig. S1: colored lines) seasonality and the difference between the two model results was used to correct the firn data for seasonality. These corrected values were used as input in the inverse model. Fig. S1 shows that the effect of seasonality is larger at NEEM than at NGR and DI, because the NEEM firn samplings occurred in the mid-summer, close to the seasonal minimum in $\delta^{13}C(CH_4)$, whereas for NGR and DI the firn samplings were carried out in spring (Fig. S1).

2. Sensitivity to uncertainties on the CH_4 scenario

Input for the model is a reconstructed atmospheric CH_4 scenario (Buizert et al., 2011). This scenario is based on direct atmospheric measurements from continuous atmospheric monitoring from the NOAA-ESRL network and from high-resolution firn/ice core measurement from the high accumulation site of Law Dome, Antarctica (Etheridge et al., 1998, Mac Farling Meure et al., 2006). As shown in

Section 5.3 of the main paper, the temporal change in the CH_4 mixing ratio is responsible for a large fraction of the $\delta^{13}C(CH_4)$ variations in the firn, because without a CH_4 trend, no diffusive fractionation would occur.

In order to evaluate more precisely the sensitivity of $\delta^{13}C(CH_4)$ to the precise shape of the CH_4 scenario, the model was forced with the minimum and maximum values of the CH_4 scenario (Buizert et al., 2011). The results depicted in Fig. S2, show that the scenarios inferred by the minimum (left panels: green line) and the maximum (left panels: purple line) CH_4 trend are within the uncertainty envelopes of our $\delta^{13}C(CH_4)$ best-guess scenario. However, the uncertainty on the CH_4 scenario affects the slope of the reconstructed $\delta^{13}C(CH_4)$ trend and may explain the difference between our results and Cape Grim air archive data.

3. Sensitivity to the regularization term

Since reconstructing atmospheric scenarios from firn air data is an under-constrained approach (less data than degrees of freedom), additional information is required to obtain a unique solution. This additional information is provided as a regularization term "k^2" which controls the smoothness of the solution (Rommelaere et al., 1997). Higher values of k^2 lead to smoother $\delta^{13}C(CH_4)$ scenarios while low values of k^2 lead to more variable solutions which fits more of the variability of firn air data (which also are associated with an analytical error). As the timescale of $\delta^{13}C(CH_4)$ variations in the atmosphere is long (Tans, 1997), the regularization term has to be chosen to yield a smooth scenario that still fits the data within the uncertainty.

In order to investigate the sensitivity of $\delta^{13}C(CH_4)$ to the regularization term, we vary it by several orders of magnitude. Fig. S3 shows the effect of increasing (left panel: blue lines) the regularization term by a factor 100 (long-dashed blue lines) and by a factor of 10 (short-dashed blue lines) and by decreasing it (left panel: green lines) by a factor 100 (long-dashed green lines) and of 10 (short-dashed green line). For the SH sites, the difference among the scenarios, long-dashed line, short-dashed line and full-line (best-guess scenario) is very small. For the NH sites, the difference is much larger, but the scenarios all fit the measurements within uncertainties, except for the early part of the profile for the factor 100 decrease. Apparently, the number of different sites constraining the model is important. For the SH, where 7 qualitatively different sites are used as input for the multi-site inversion, the regularization term does not affect the $\delta^{13}C(CH_4)$ scenario significantly, whereas for the NH with only 4 sites with very similar profiles the scenario is less well constained.

4. Deep firn data

In the multisite scenario reconstruction, the deepest data-points at each site were excluded, because the correction for isotopic fractionation is very uncertain (Buizert et al., 2011) in the deep firn. Two different way of excluding the data were used. First, removing the data showing strong deviation with the modeled isotopic fractionation in firn (Fig. 5 main paper and Fig. S4, black lines) and second removing all data below the lock-in depth (Witrant et al., 2011) (Fig. S4, red and green lines). Both methods show very similar results.

SUPPLEMENTARY REFERENCES

Buizert, C. et al.: Gas transport in firn: multiple-tracer characterization and model intercomparison for NEEM, Northern Greenland, Atmos. Chem. Phys. Discuss. 11, 15975, 2011.

Dlugokencky, E. J., Bruhwiler, L., White, J. W. C., Emmons, L. K., Novelli, P. C., Montzka, S. A., Masarie, K. A., Lang, P. M., Crotwell, A. M., Miller, J. B., and Gatti, L. V.: Observational constraints on recent increases in the atmospheric CH_4 burden, Geophys. Res. Lett., 36, L18803, DOI:18810.11029/12009gl039780, 2009.

Etheridge, D. M., Steele, L. P., Francey, R. J., and Langenfelds, R. L.: Atmospheric CH_4 between 1000 AD and present: Evidence of antropogenic emissions and climatic variability, J. Geophys. Res., 103, 15979-15993, 1998.

MacFarling Meure, C., Etheridge, D., Trudinger, C., Steele, P., Langenfelds, R., Ommen, T. v., Smith, A., and Elkins, J.: Law Dome CO_2, CH_4 and N_2O ice core records extended to 2000 years BP Geophys. Res. Lett., 33, L14810, DOI:14810.11029/12006GL026152, 2006.

Miller, J. B., Mack, K. A., Dissly, R., White, J. W. C., Dlugokencky, E. J., and Tans, P. P.: Development of analytical methods and measurements of $\delta^{13}C$ in atmospheric CH_4 from the NOAA/CMDL global air sampling network, J. Geophys. Res., 107, 4178, DOI: 10.1029/2001JD000630, 2002.

Rommelaere, V., Arnaud, L., and Barnola, J.-M.: Reconstructing recent atmospheric trace gas concentrations from polar firn and bubbly ice data by inverse methods, J. Geophys. Res., 102, 30 069–30 083, 1997.

Tans, P. P.: A note on isotopic ratios and the global atmospheric methane budget, Gl. Biogeochem. Cycles, 11, 77-81, 1997.

Tyler, S. C., Rice, A. L., and Ajie, H. O.: Stable isotope ratios in atmospheric CH_4: Implications for seasonal sources and sinks, J. Geophys. Res., 112, D03303, DOI:10.1029/2006JD007231, 2007.

Wang, Z., Chappellaz, J., Martinerie, P., Park, K., Petrenko, V., Witrant, E., Blunier, T., Brenninkmeijer, C. A. M., and Mak, J. E.: The isotopic record of Northern Hemisphere atmospheric carbon monoxide since 1950, implications for the CO budget, Atmos. Chem. Phys. Discuss., 11, 30627-30663, doi:10.5194/acpd-11-30627-2011, 2011.

Witrant, E., Martinerie, P., , Hogan, C., Laube, J. C., Kawamura, K., Capron, E., Montzka, S. A., Dlugokencky, E. J., Etheridge, D., Blunier, T., and Sturges, W. T.: A new multi-gas constrained model of trace gas non-homogeneous transport in firn: evaluation and behavior at eleven polar sites, Atmos. Chem. Phys. Discussions, 11, 23 029–23 080,

doi:10.5194/acpd-11-23029-2011, 2011.

FIGURES

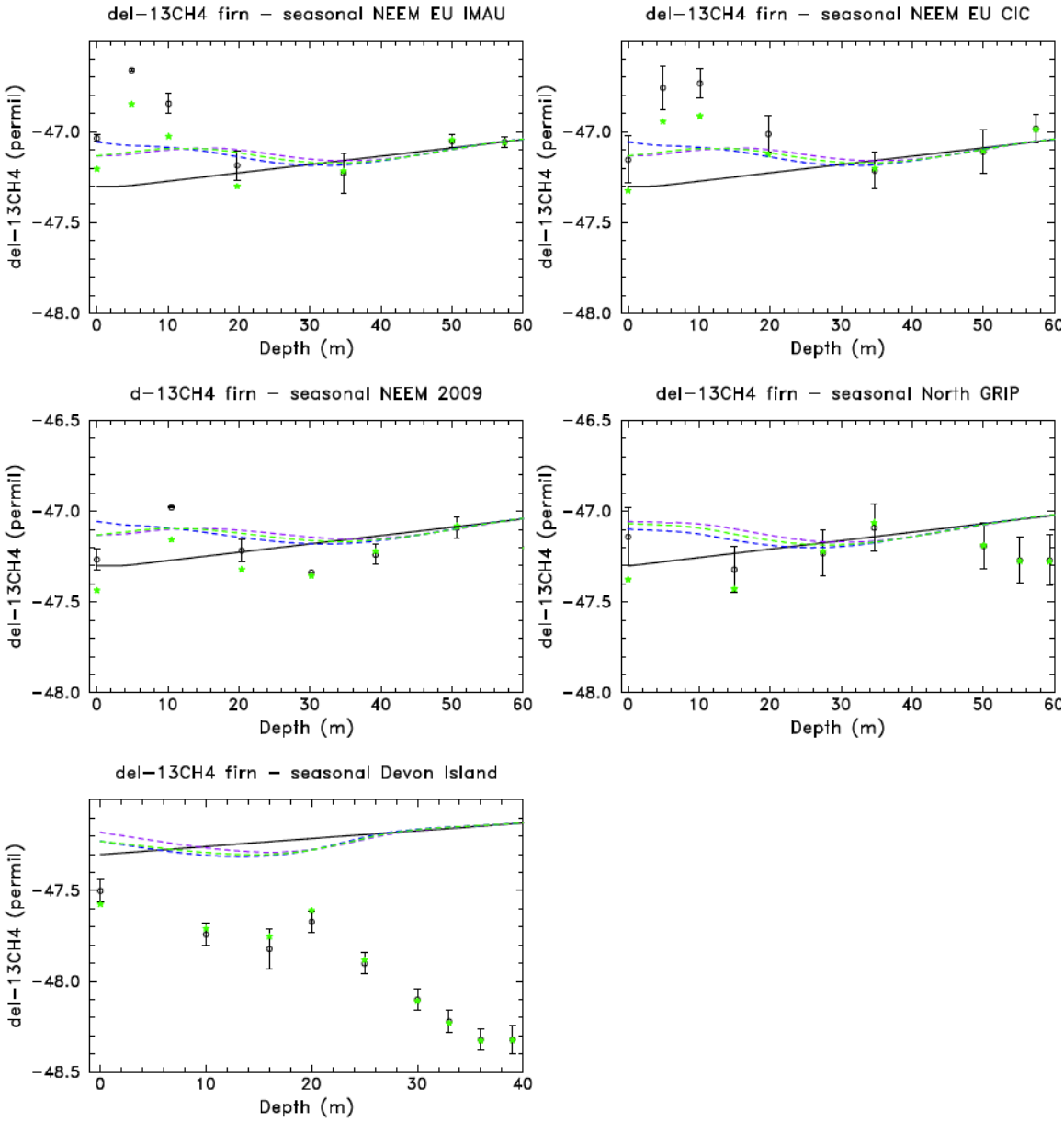

Figure S1: Model estimate of the effect of seasonality on $\delta^{13}C(CH_4)$ in firn. Measured isotopic ratios are shown as black circles with error bars. Simulated values with constant atmospheric trends in $\delta^{13}C(CH_4)$ and without seasonal cycle are plotted as black lines, simulated values with constant atmospheric trends and perpetual mean seasonal cycle are plotted as green dashed lines. The increasing isotopic ratios with depth obtained from constant scenarios (black lines) illustrate the effect of gravitational fractionation. The purple and blue dashed lines illustrate the effect of shifting the final date of the simulation (drill date) by plus or minus 15 days respectively. The green dots are the measurement values corrected for the difference between the black solid lines (no seasonality) and black dashed lines (with seasonality)

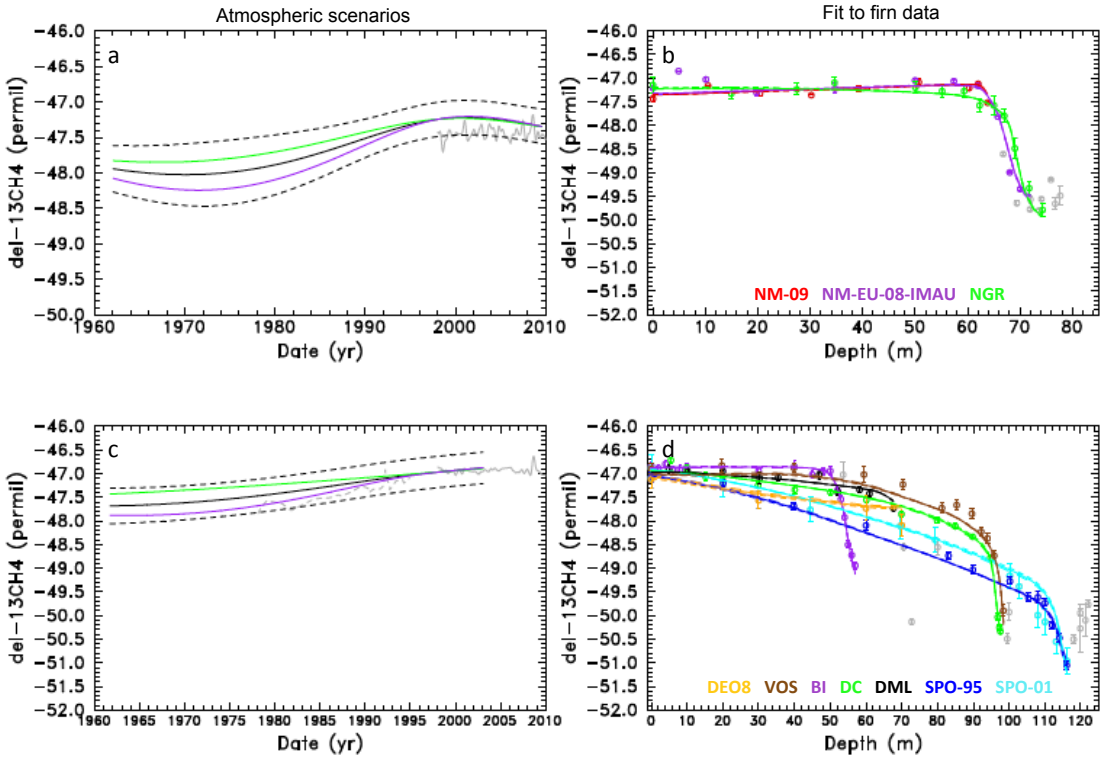

Figure S2: Multi-site $\delta^{13}C(CH_4)$ trend reconstructions (left) and their match to the firn data (right) in the NH (top) and SH (bottom). Left panels: Minimum (green) maximum (purple) or best estimate (black) CH_4 scenario with uncertainty limits (dashed lines) as described by Buizert et al., 2011. Right panels: Isotope profiles at NM-EU-08 (purple), NM-09 (red), NGR (green) and DI (black) for the NH and DE08 (orange), BI(purple), SPO-95 (dark blue), SPO-01 (light blue), DML (black), DC (green), VOS (brown) for the SH. Equal weight is given to all sites and for SPO-01 the diffusivity from SPO-95 is used.

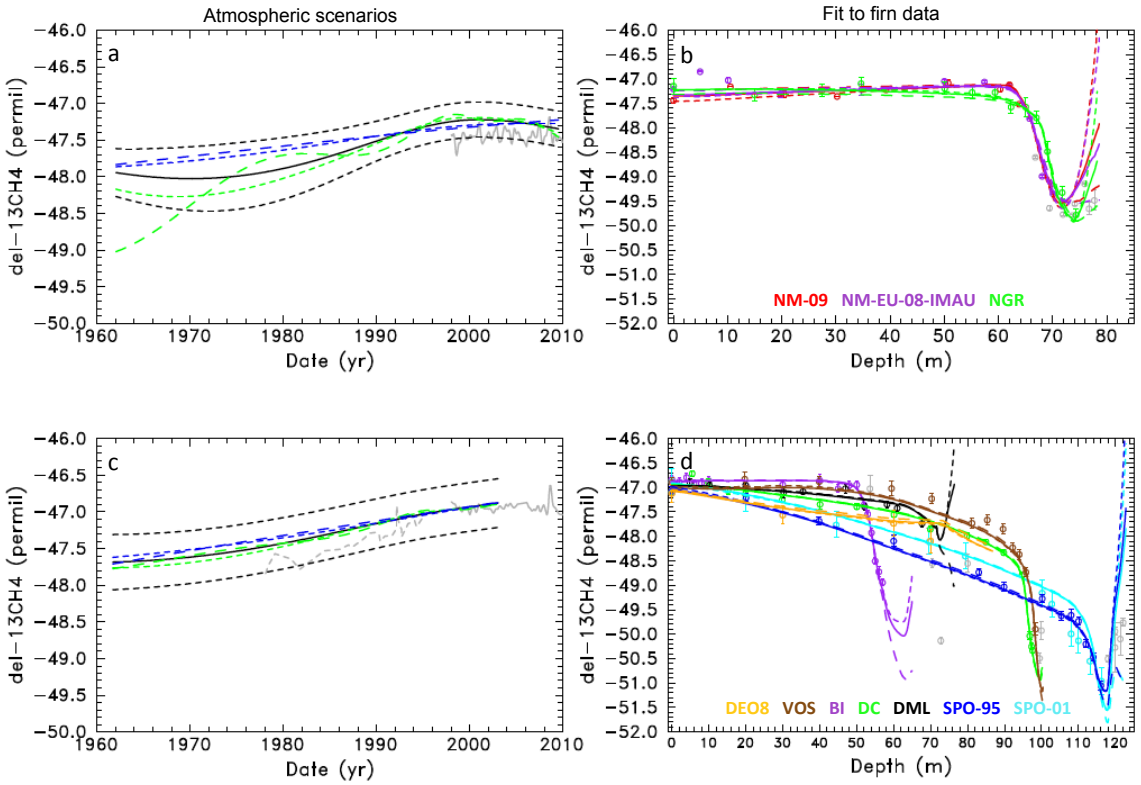

Figure S3: Sensitivity of $\delta^{13}C(CH_4)$ reconstructions to the regularization term. Multi-site $\delta^{13}C(CH_4)$ trend reconstructions (left panels) and their match of the firn data (right panels). a: regularization term increased by a factor of 100 (long-dashed blue line), regularization term increased by a factor of 10 (short-dashed blue line), regularization term reduced by a factor of 100 (long-dashed green line) and regularization term reduced by a factor of 10 (short-dashed green line). c: regularization term reduced by a factor of 100 (short-dashed lines), regularization term increased by a factor of 100 (long-dashed lines) compare with the data. North hemisphere sites (upper panel): NM-EU-08 (purple), NM-09 (red), NGR (green) and DI (black). South hemisphere sites (lower panel): DE08 (orange), BI(purple), SPO-95 (dark blue), SPO-01 (light blue), DML (black), DC (green), VOS (brown). Equal weight for all sites and modified diffusivity for SPO-01 (using diffusivity from SPO-95) were used.

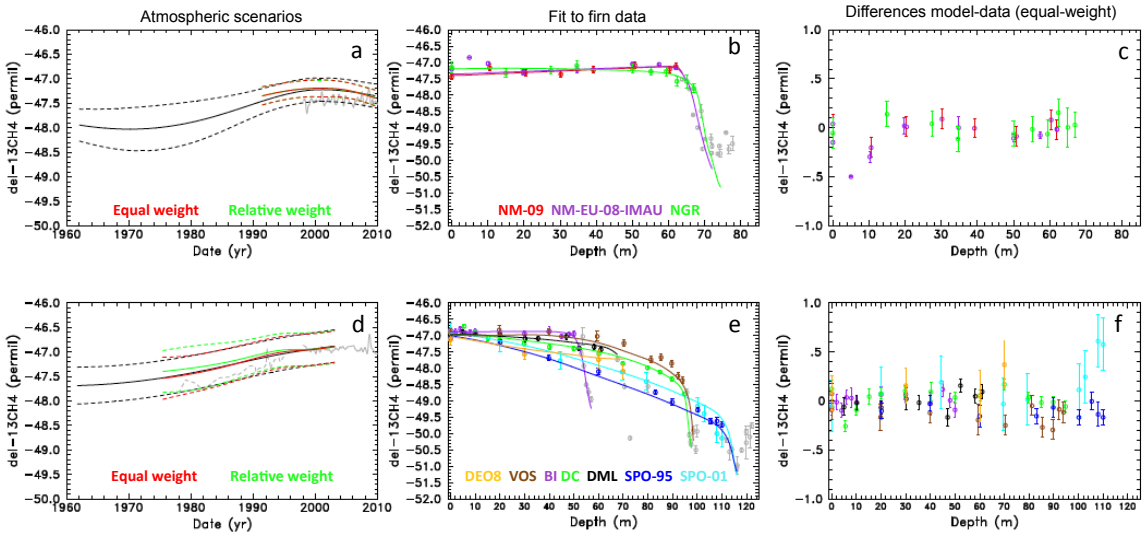

Figure S4: Multi-site $\delta^{13}C(CH_4)$ trend reconstructions (a and d), the fit to the firn data (b and e) and the difference between model-data (c and f) . NH sites (a, b and c) and SH sites (d, e and f). Multi-site inversion with equal-weight for each site (red dashed line) and with single site RMS difference based weight for each site (green dashed line) (left panels). The grey curve (left panel) represents air-archive from Cape Grim (Francey et al., 1998) and continuous atmospheric monitoring data from the NOAA-ESRL network. This figure is very similar than the Fig. 5 (the black line on panels a and b represent the red line in Fig. 5) of the main paper, but here all points below the lock-in depth are excluded so the scenarios are shorter.